

GALAXY CLUSTERS IN FORMATION: DETERMINING THE AGE OF THE RED-SEQUENCE IN OPTICAL AND X-RAY CLUSTERS AT $z \sim 1$ WITH HST¹

BENJAMIN P. KOESTER^{2,3}, MICHAEL D. GLADDERS^{2,3,4}, DAVID G. GILBANK⁵, H.K.C. YEE⁶, KYLE BARBARY^{7,8}, KYLE S. DAWSON^{7,9}, JOSHUA MEYERS^{7,8}, SAUL PERLMUTTER^{7,8}, DAVID RUBIN^{7,8}, NAO SUZUKI⁷

Draft version October 18, 2021

ABSTRACT

Using deep two-band imaging from the *Hubble Space Telescope*, we measure the color-magnitude relations (CMR) of E/S0 galaxies in a set of 9 optically-selected clusters principally from the Red-Sequence Cluster Survey (RCS) at $0.9 < z < 1.23$. We find that the mean scatter in the CMR in the observed frame of this set of clusters is 0.049 ± 0.008 , as compared to 0.031 ± 0.007 in a similarly imaged and identically analyzed X-ray sample at similar redshifts. Single-burst stellar population models of the CMR scatter suggest that the E/S0 population in these RCS clusters truncated their star-formation at $z_l \simeq 1.6$, some 0.9 Gyrs later than their X-ray E/S0 counterparts which were truncated at $z_l \simeq 2.1$. The notion that this is a manifestation of the differing evolutionary states of the two populations of cluster galaxies is supported by comparison of the fraction of bulge-dominated galaxies found in the two samples which shows that optically-selected clusters contain a smaller fraction of E/S0 galaxies at the their cores.

Subject headings:

1. INTRODUCTION

The color-magnitude relation (CMR) in galaxies in the cores of galaxy clusters is a fossil record of the integrated star-formation histories of the constituent galaxies (see Renzini 2006, for a review). The slope of the CMR encodes the build-up of the mass-metallicity relation, while its scatter is thought to reflect the variation in the formation epochs of the cluster galaxies (Kodama & Arimoto 1997; Kauffmann & Charlot 1998; Bernardi et al. 2005).

Mounting observational data has culminated in a picture of galaxy formation that attempts to explain the conversion of star-forming “blue-cloud” galaxies into passively-evolving “red-sequence” galaxies (e.g., Faber et al. 2007; Mei et al. 2009). This picture cites some combination of the quenching of star formation in the blue-cloud and the merging of already red galaxies as driving the build-up of the red-sequence.

The high resolution imaging delivered by HST/ACS plays an important role in disentangling these effects, as it allows color measurements even for faint galaxies,

and robust morphological measurements, which include either manual classification of E, S0, Sp, and Irr (e.g., Postman et al. 2005) or automated separation of E/S0 types from later types (e.g., Abraham et al. 2007). In particular, combined color and morphological data can be used to measure the color scatter of the E/S0 galaxies in the CMR, which places constraints on the formation epochs of stars in cluster galaxies (e.g., Bower et al. 1992).

Until now, $z \sim 1$ systematic space-based studies of the CMR in the cores of galaxy clusters have been conducted almost exclusively using a handful of X-ray selected galaxy clusters (van Dokkum et al. 1998, 2000; Blakeslee et al. 2003; Mei et al. 2006; Blakeslee et al. 2006; Mei et al. 2009). The consensus picture from these studies is that stars in these galaxies were formed at $z \gtrsim 2$.

In this Letter, we present the first precision statistical measurements of the scatter of the CMR in an optically-selected sample of galaxy clusters at $z \sim 1$. Where necessary, we adopt a flat, $\Omega_m = 0.30$ cosmology with $H_0 = 70$ km s⁻¹ Mpc⁻¹.

2. DATA

Imaging for this study was acquired as part of the *HST* Cluster SN Survey Program (Program Number 10496, PI: Perlmutter). Nine optically-selected clusters were imaged at various telescope roll angles for a total of 5000-16000s with the Advanced Camera for Surveys (ACS) on multiple visits (375s-500s per sub-exposure) in z_{850} (F850LP) and for 1000-8000s in i_{775} (F775W) (Dawson et al. 2009). Eight clusters are derived from the Red-Sequence Cluster Survey (RCS, Gladders & Yee 2005), and the ninth, XLSS J0223.0+0436, was originally included in this sample as an IR-detected cluster from the SpARCS survey (Muzzin et al. 2008; Wilson et al. 2008), but had previously been detected in both the IR (Andreoni et al. 2005) and X-ray (Pierre et al. 2004). We consider it here as an optical-IR detected cluster.

¹ Based on observations made with the NASA/ESA Hubble Space Telescope and obtained from the data archive at the Space Telescope Institute. STScI is operated by the Association of Universities for Research in Astronomy, Inc. under the NASA contract NAS 5-26555. The observations are associated with program 10496

² Department of Astronomy and Astrophysics, University of Chicago, Chicago IL 60637, USA

³ Kavli Institute for Cosmological Physics, The University of Chicago, Chicago IL 60637, USA

⁴ Visiting Associate, Observatories of the Carnegie Institution of Washington, Pasadena, CA 91101

⁵ Department of Physics and Astronomy, University of Waterloo, Waterloo ON, Canada, N2L 3G1

⁶ Department of Astronomy and Astrophysics, University of Toronto, Toronto, ON, Canada, M5S 3H4

⁷ E.O. Lawrence Berkeley National Lab, 1 Cyclotron Rd., Berkeley, CA, 94720

⁸ Department of Physics, University of California Berkeley, Berkeley, CA, 94720

⁹ Department of Physics and Astronomy, University of Utah, Salt Lake City, UT, 84112

With the exception RCSJ J0337.8-2844 an extensive spectroscopic program has obtained 5-30 confirmed spectroscopic members per cluster, enough to compute a velocity dispersion in many cases (Gilbank et al. 2008; Hicks et al. 2008; Gilbank et al. 2009). Three of the X-ray selected clusters, analyzed most recently in Mei et al. (2009) are taken from (Rosati et al. 1998), and the WARPS cluster was first presented in (Perlman et al. 2002).

Images for each cluster were coadded using Multidrizzle (Koekemoer et al. 2002), with a Gaussian kernel, $\text{pixfrac} = 0.8$, and a final output pixel size of 0.03 arcsec/pixel. The detailed photometric and morphological pipelines developed for this work are described and tested in detail in Koester et al. (2009). In brief, object detection was performed with SExtractor (Bertin & Arnouts 1996), and the resulting catalogs were manually cleaned of diffraction spikes, pupil ghosts, and saturated stars. The final galaxy catalog was distilled from the full catalog following Leauthaud et al. (2007). Total magnitudes are taken as `MAG_AUTO` magnitudes with a correction applied (e.g., Bernstein et al. 2002a,b; Benítez et al. 2004; Blakeslee et al. 2006) appropriate for E galaxies. As noted in Blakeslee et al. (2003), the differential smearing of the PSF between i_{775} and z_{850} makes the PSF approximately 10% broader in z_{850} . We correct this using a PSF matching scheme that places both the i_{775} and z_{850} images on the same footing by convolving the latter image with the PSF of the former, and vice-versa.

The PSF model was built in each bandpass using the SExtractor `MU_MAX - MAG_AUTO` parameters to select acceptable PSF stars in the coadded images, which were then visually checked. In a circularly symmetric $\sim 1'$ radius, a single PSF model adequately describes the aggregate distortion realized in the final image due to HST/ACS optics and temporal variations thereof (Jee et al. 2007; Rhodes et al. 2007), charge diffusion (Krist et al. 2003), the so-called red-halo effect (Sirrianni et al. 2005; Jee et al. 2007), and the drizzling process. For the precision photometry required in this study, this necessarily restricts us to considering the inner $500h^{-1}$ kpc of each cluster, where the PSF is approximately constant, and the convolutions required for PSF-matching are minimally position dependent.

In the coadded and convolved z_{850} image of each cluster, we construct adaptively-determined apertures with GALFIT (Peng et al. 2002) by fitting Sersic profiles constrained to $1 \leq n \leq 4$, thus returning an estimate of an effective radius, R_e for each object. Nearby objects ($\leq 3R_e$) are simultaneously fit, and all remaining objects within $6R_e$ are masked, and the sky estimated as in Häussler et al. (2007). The same aperture is applied in the i_{775} band to measure the $i_{775} - z_{850}$ color. Errors on the aperture magnitudes are determined for each galaxy by comparing the repeat observations of objects as a function of magnitude. Typical errors range from 0.02 mags at $z_{850} = 21$ to 0.05 magnitudes at $z_{850} = 24$.

We use an automated scheme, MORPHEUS (Abraham et al. 2007) to separate E/S0 galaxies from the irregulars and spirals, taking objects with a Gini coefficient > 0.45 and asymmetry parameter < 0.1 to be E/S0 galaxies. Because z_{850} stays redward of the 4000\AA break until $z \sim 1.3$, the signal-to-noise

ratio (S/N) for early-type galaxies remains considerable. Based on comparison to the manual classifications for RDCS J1252.9-2927 in Postman et al. (2005), the E/S0 galaxies we classify at $z = 1.24$ comprise a 90% pure and complete sample.

3. MEASURING THE COLOR-MAGNITUDE RELATION

Color-magnitude diagrams were created for each cluster, and the red-sequence color limits were determined by eye. Objects falling within these broad limits ($\simeq 3\sigma$ of the final best-fit line) with luminosities greater than $0.3L_*$ ($z_{850} = 24$ at $z = 1.24$) were taken to be the red-sequence. The luminosity limit is strictly chosen to be bright enough to ensure the morphological classifications are robust. A line was fit to E/S0 objects within these bounds using a simple least-squares method, and was sigma-clipped at 3σ in $i - z$ color. This was iterated until convergence to derive the slope and zero point of the best-fit line, and the scatter of E/S0 objects (including the rejected outliers) about this line was computed using a bi-weight estimator of scale (Beers et al. 1990).

The best-fit slopes of two clusters, RCS J2156.7-0448 and RCS J2345.4-3632, are not robust to the color cuts used, due largely to the relative paucity of E/S0 galaxies at the faint end of their CMRs ($z_{850} > 22.5$). We thus fix the slope for these clusters at -0.05 and the reported scatter is measured about this line; the resulting scatter about the best-fit line varies by only ~ 0.015 mags depending on the line used.

To assess uncertainties, we run 1000 bootstrap resamples on each cluster, and compute the mean and standard error of the red sequence fits to these resamples. There is a further contribution to scatter due to photometric error. Using the method of Stanford et al. (1998) we find that it contributes no more than 0.01-0.02 magnitudes in quadrature to the measured scatter; we correct the measured scatters accordingly.

Finally, we note that the derived CMR is measured inside a fixed $0.5 h^{-1}$ Mpc cluster-centric radius, the approximate observed field-of-view of most of these observations. We do not attempt to compute R_{200} or any other scale radius, which would require additional dynamical data, X-ray data, or possibly wider field images (e.g., Rozo et al. 2008).

4. THE CMR IN $z \sim 1$ RCS CLUSTERS

Table 1 shows the measured CMRs for our 9 optically-selected clusters and also our own measurements of a subset of archival X-ray selected clusters also measured in i_{775} and z_{850} . The Table also displays $N_{E/S0}$, the number of E/S0 galaxies used in measuring the CMR, and a richness $N_{0.5}$, which is the number of red-sequence galaxies brighter than $0.3L_*$, within $0.5h^{-1}$ Mpc of the BCG. RCS J0337.8-2844 and RCS J2156.7-0448, the two least rich clusters, exhibit the largest scatter. RCS J2319.8+0038 and RCS J0439.6-2904, which are both X-ray detected (Hicks et al. 2008; Gilbank et al. 2008), and the X-ray selected clusters have relatively high $N_{0.5}$ richnesses.

In this Letter, we focus on the distribution of scatters. In the observed frame, it is apparent that the optical and X-ray samples have discordant average scatters in observed $i_{775} - z_{850}$: the optical sample, at 0.049 ± 0.008 is nearly 50% larger than the X-ray scatter at 0.031 ± 0.007 .

A t -test of the means of the two samples rejects the null hypothesis that the two samples come from the same underlying population at the 95% level.

The scatter is thought to reflect variations in galaxy formation time (but see Menci et al. 2008). It has thus been modeled using Bruzual-Charlot single-burst models (Bruzual & Charlot 2003), which posit that all the stars in a given galaxy are formed in a coeval burst at some redshift, z_f , and evolve passively thereafter. The scatter in the CMR results from the variation in formation times for the constituent galaxies that have formed in single bursts between reionization, z_r , and some lower redshift, z_l .

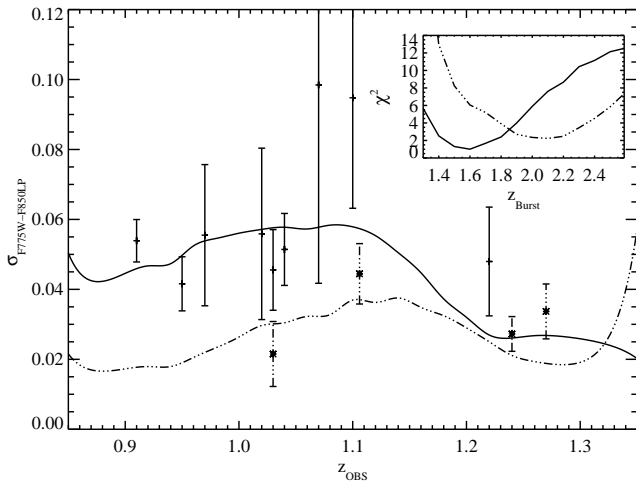


FIG. 1.— Bruzual-Charlot Single-Burst Models of the Scatter. Given the cluster redshift, z_{obs} , stars with error bars represent the scatter of the red-sequence in X-ray selected clusters, while the normal crosses and errors show the scatters for the optically-selected clusters. The best-fit Bruzual-Charlot single-burst models for the X-ray and optical samples are shown as dashed and solid lines, respectively. Inset: χ^2 minimization for the X-ray and optical models, indicating the lowest redshift, z_{burst} , of the epoch during which galaxies formed. The two samples clearly favor different minima in the context of this model. Alternatively, taking $z_{burst} = 1.6$ in the x-ray sample, the $\chi^2 = 6.1$, a result that is discordant with the optically-selected best-fit $z_{burst} = 2.1$ model at the few sigma level.

Using the ACS i_{775} and z_{850} response curves as described in Sirianni et al. (2005), we determine the expected observed scatter in $i_{775} - z_{850}$ using a single-burst spectrum, following the Monte Carlo method first described in van Dokkum et al. (1998). Assuming a galaxy formed at some redshift, z_f , we create 10,000 “galaxies” by drawing from a random uniform formation age distribution corresponding to a redshift range of $z_l \leq z_f \leq z_r$. For each z_l , the last redshift at which galaxies formed, the model predicts a scatter in $i_{775} - z_{850}$ that would be observed at some redshift, z_{obs} . For a given set of clusters, we then choose the best-fit model by minimizing χ^2 :

$$\chi^2 = \sum \frac{(\sigma_{iz}^{mod} - \sigma_{iz}^{obs})^2}{\sigma_{err}^2}, \quad (1)$$

where the “mod” and “obs” superscripts refer to the predicted model and observed data scatters, and σ_{err} is the error on each observed σ_{obs} . In Figure 1, we show the result of this process for both the optical (solid) and X-ray

(dashed) samples. The optical sample favors $z_l = 1.6$, and the X-ray sample favors $z_l = 2.1$, suggesting that the E/S0 galaxies on the red-sequence in X-ray selected clusters ended their star formation some 0.9 Gyr earlier.

5. DISCUSSION

The small number of E/S0 galaxies, $N_{E/S0}$, in some of the less rich clusters highlights a possible concern. Simple Monte Carlo simulations of random draws from a normal distribution indicate that at $N = 10$, even the bi-weight estimator of scale returns a scatter that is biased high by 10%; this is reduced to 3% by $N = 20$, and $\lesssim 1\%$ at $N=40$. Contamination by non-cluster members also contributes to scatter. Randomly adding a single galaxy that passes the red-sequence color cuts adds as much as an additional 10% bias at $N = 10$. Fortunately, our analysis of the GOODS⁹ (Giallisco et al. 2004) fields indicate that the average background (for morphologically selected galaxies passing our color and luminosity cuts) is $\lesssim 1$ galaxy.

Another concern is line-of-sight projection of large structures. RCS J0439.6-2904 is known to show two redshift peaks at $z = 0.9435$ and $z = 0.9681$ (Gilbank et al. 2007; Cain et al. 2008), for a separation of $\simeq 7000$ km s⁻¹. A cursory analysis of the halo catalogs from the VIRGO simulations (Evrard et al. 2002) shows that halo-halo projections of this sort are expected in about $\simeq 10 - 20\%$ of RCS clusters in this mass range at $z \sim 1$; a similar value is found in spectroscopic data (Gilbank et al. 2007). At such a separation, Monte Carlo simulations show that two projected halos each with $\sigma_v = 1000$ km s⁻¹ have a resultant measured scatter inflated by only 0.003 magnitudes, which has no significant effect on our results.

Spectroscopy does not yet exist for RCS J0337.8-2844 and spectroscopic confirmation is pending. Only limited spectroscopy exists for RCS J2156.7-0448 (5 confirmed spectroscopic members), and its measured X-ray flux is consistent with zero (Hicks et al. 2008), although the strong lensing in this system (Gladders et al. 2003) indicates that its mass is cluster scale. Regardless, we find that removing one or both of these clusters does not affect our conclusions. The other seven clusters are robustly spectroscopically confirmed (Gilbank et al. 2009).

For three of the X-ray clusters (all except WARP J1415.1+3612), Mei et al. (2009) place constraints on z_l with single-burst models, using a combination of HST data, manual morphological measurements, and spectroscopic confirmation where available. They generally find formation epochs of $z_l \simeq 2.2$, only slightly higher than our own measurements. As part of the validation process of our pipeline, we compare our measured CMR parameters in these 3 X-ray clusters with previous work, and find that they agree within errors.

For the 4 optical clusters in this study that have velocity dispersion estimates, we find the distribution of velocity dispersions is similar to the X-ray sample, with the RCS clusters having $670 \lesssim \sigma_v \lesssim 1080$ km s⁻¹, and the X-ray sample $650 \lesssim \sigma_v \lesssim 747$ km s⁻¹. The number of

⁹ Based on observations made with the NASA/ESA Hubble Space Telescope, obtained from the data archive at the Space Telescope Institute. STSci is operated by the Association of Universities for Research in Astronomy, Inc. under the NASA contract NAS 5-26555. The observations are associated with program 9425.

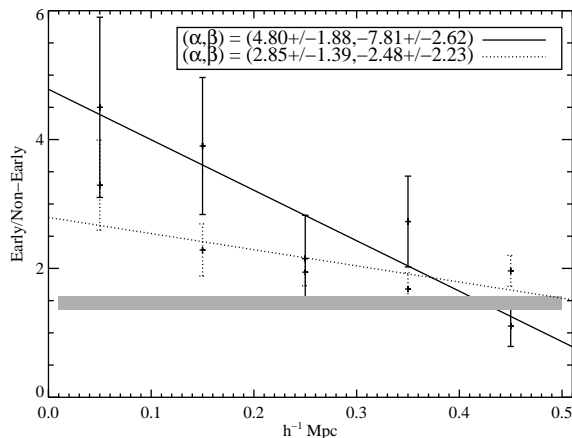


FIG. 2.— Radial Dependence of E/S0 Fraction. X-ray selected clusters (solid) show a larger fraction of color-selected E/S0 galaxies than optically-selected (dotted) clusters, and both fractions approximately converge to the GOODS field values (gray bar) by $0.5 h^{-1}$ Mpc. Best-fit regression lines are overplotted as well, and the intercept and slope (α, β) are shown in the legend. The X-ray fraction at $r \leq 0.4 h^{-1}$ Mpc is consistent with that measured in (Postman et al. 2005).

E/S0 galaxies (Table 1) suggests that the clusters in the X-ray sample are as rich as the richest optical clusters, and a t -test reveals no significant difference between richnesses of the two samples. Additionally, the fact that we have run the same automated pipeline on all the clusters rules out systematic differences that might be expected in measurements conducted in different studies, or in different bandpasses.

The observed difference in red-sequence scatters between the two samples therefore suggests that the galaxy populations in the clusters themselves are different. To test this further, we measure the composite red-sequence bulge-dominated (E/S0) fraction in each sample as a function of cluster-centric radius, shown in Figure 2. Both samples reach the GOODS field value by $0.5 h^{-1}$ Mpc. Overplotted are best-fit regression lines estimated using `linmix_err` (Kelly 2007), which both exhibit a significant correlation of the fraction with radius. The regression parameters themselves (Figure 2, legend) disagree at the $\approx 2\sigma$ level. This suggests that E/S0 galaxies form a larger fraction of the cores of X-ray clusters,

and fall off faster than the optical clusters before reaching the field value. At lower redshifts the development of the morphology-density relation, particularly through the build-up of S0 galaxies on the red sequence, appears correlated with cluster age (Dressler et al. 1997), and so these differences also suggest that the optical clusters are younger. We note however that the radii in Figure 2 are metric, and it is not clear that these trends would be mitigated by the use of an aperture scaled to the virial radius. The similarity of the X-ray and optical velocity dispersions is, however, evidence that the virial radii are similar.

The measurements presented in this study have consequences for studies of cluster evolution and galaxy formation. Distant optically-selected clusters likely represent a younger state of massive halos compared to their X-ray selected counterparts. If cluster galaxies from the most highly-biased regions of the Universe formed earlier in the X-ray sample, as suggested by our analysis, one might be tempted to conclude that the clusters themselves collapsed earlier, and that the presence of a hot ICM reflects this more evolved state. In this scenario, X-ray selected clusters only represent a subset of the most massive halos at $z \sim 1$, and optical samples fill out the part of the mass function that is younger, and not X-ray bright. However, absent X-ray data for the full optical sample, it is difficult to draw any definite conclusions on the relationship of cluster dynamical evolution to X-ray luminosity and the red-sequence.

We thank Keren Sharon for a critical reading of the manuscript, and Gus Evrard and Jiangang Hao for helpful discussions. Financial support for this work was provided by NASA through program GO-10496 from the Space Telescope Science Institute, which is operated by AURA, Inc., under NASA contract NAS 5-26555. This work was also supported in part by the Director, Office of Science, Office of High Energy and Nuclear Physics, of the U.S. Department of Energy under Contract No. AC02-05CH11231.

REFERENCES

- Abraham, R. G. et al. 2007, *ApJ*, 669, 184
 Andreon, S., Valtchanov, I., Jones, L. R., Altieri, B., Bremer, M., Willis, J., Pierre, M., & Quintana, H. 2005, *MNRAS*, 359, 1250
 Beers, T. C., Flynn, K., & Gebhardt, K. 1990, *AJ*, 100, 32
 Benítez, N. et al. 2004, *ApJS*, 150, 1
 Bernardi, M., Sheth, R. K., Nichol, R. C., Schneider, D. P., & Brinkmann, J. 2005, *AJ*, 129, 61
 Bernstein, R. A., Freedman, W. L., & Madore, B. F. 2002a, *ApJ*, 571, 56
 —. 2002b, *ApJ*, 571, 107
 Bertin, E., & Arnouts, S. 1996, *A&AS*, 117, 393
 Blakeslee, J. P. et al. 2003, *ApJ*, 596, L143
 —. 2006, *ApJ*, 644, 30
 Bower, R. G., Lucey, J. R., & Ellis, R. S. 1992, *MNRAS*, 254, 589
 Bruzual, G., & Charlot, S. 2003, *MNRAS*, 344, 1000
 Cain, B. et al. 2008, *ApJ*, 679, 293
 Dawson, K. S. et al. 2009, in prep
 Dressler, A. et al. 1997, *ApJ*, 490, 577
 Evrard, A. E. et al. 2002, *ApJ*, 573, 7
 Faber, S. M. et al. 2007, *ApJ*, 665, 265
 Giavalisco, M. et al. 2004, *ApJ*, 600, L93
 Gilbank, D. G., Yee, H. K. C., Ellingson, E., Gladders, M. D., Barrientos, L. F., & Blindert, K. 2007, *AJ*, 134, 282
 Gilbank, D. G., Yee, H. K. C., Ellingson, E., Hicks, A. K., Gladders, M. D., Barrientos, L. F., & Keeney, B. 2008, *ApJ*, 677, L89
 Gilbank, D. G. et al. 2009, in prep
 Gladders, M. D., Hoekstra, H., Yee, H. K. C., Hall, P. B., & Barrientos, L. F. 2003, *ApJ*, 593, 48
 Gladders, M. D., & Yee, H. K. C. 2005, *ApJS*, 157, 1
 Häussler, B. et al. 2007, *ApJS*, 172, 615
 Hicks, A. K. et al. 2008, *ApJ*, 680, 1022
 Jee, M. J., Blakeslee, J. P., Sirianni, M., Martel, A. R., White, R. L., & Ford, H. C. 2007, *PASP*, 119, 1403
 Kauffmann, G., & Charlot, S. 1998, *MNRAS*, 294, 705
 Kelly, B. C. 2007, *ApJ*, 665, 1489
 Kodama, T., & Arimoto, N. 1997, *A&A*, 320, 41

- Koekemoer, A. M., Fruchter, A. S., Hook, R. N., & Hack, W. 2002, in The 2002 HST Calibration Workshop : Hubble after the Installation of the ACS and the NICMOS Cooling System, Proceedings of a Workshop held at the Space Telescope Science Institute, Baltimore, Maryland, October 17 and 18, 2002. Edited by Santiago Arribas, Anton Koekemoer, and Brad Whitmore. Baltimore, MD: Space Telescope Science Institute, 2002., p.337, ed. S. Arribas, A. Koekemoer, & B. Whitmore, 337–+
- Koester, B. P. et al. (2009), in prep
- Krist, J. E., Hartig, G. F., Clampin, M., Golimowski, D. A., Ford, H. C., & Illingworth, G. D. 2003, Advanced camera for surveys coronagraph on the Hubble Space Telescope
- Leauthaud, A. et al. 2007, ApJS, 172, 219
- Mei, S. et al. 2009, ApJ, 690, 42
- . 2006, ApJ, 644, 759
- Menci, N., Rosati, P., Gobat, R., Strazzullo, V., Rettura, A., Mei, S., & Demarco, R. 2008, ApJ, 685, 863
- Muzzin, A. et al. 2008, ArXiv e-prints
- Peng, C. Y., Ho, L. C., Impey, C. D., & Rix, H.-W. 2002, AJ, 124, 266
- Perlman, E. S., Horner, D. J., Jones, L. R., Scharf, C. A., Ebeling, H., Wegner, G., & Malkan, M. 2002, ApJS, 140, 265
- Pierre, M. et al. 2004, Journal of Cosmology and Astro-Particle Physics, 9, 11
- Postman, M. et al. 2005, ApJ, 623, 721
- Renzini, A. 2006, ARA&A, 44, 141
- Rhodes, J. D. et al. 2007, ArXiv Astrophysics e-prints
- Rosati, P., della Ceca, R., Norman, C., & Giacconi, R. 1998, ApJ, 492, L21+
- Rozo, E. et al. 2008, ArXiv e-prints
- Sirianni, M. et al. 2005, PASP, 117, 1049
- Stanford, S. A., Eisenhardt, P. R., & Dickinson, M. 1998, ApJ, 492, 461
- van Dokkum, P. G., Franx, M., Fabricant, D., Illingworth, G. D., & Kelson, D. D. 2000, ApJ, 541, 95
- van Dokkum, P. G., Franx, M., Kelson, D. D., Illingworth, G. D., Fisher, D., & Fabricant, D. 1998, ApJ, 500, 714
- Wilson, G. et al. 2008, in Astronomical Society of the Pacific Conference Series, Vol. 381, Infrared Diagnostics of Galaxy Evolution, ed. R.-R. Chary, H. I. Teplitz, & K. Sheth, 210–+

TABLE 1
CLUSTERS AND CMR PARAMETERS USED IN THIS STUDY

Name ¹	$N_{E/S0}$	z_{spec}	$(i - z)$ slope	$(i - z)$ scatter	$N_{0.5}$ ²
RCS J2319.8+0038	39	0.91	-0.066 ± 0.012	0.054 ± 0.006	57.6 ± 1.3
RCS J0439.6-2904	23	0.95	-0.053 ± 0.019	0.042 ± 0.008	23.3 ± 0.9
RCS J1511.0+0903	12	0.97	-0.035 ± 0.053	0.055 ± 0.020	9.4 ± 1.0
RCS J0221.4-0321	18	1.02	-0.042 ± 0.073	0.056 ± 0.025	26.9 ± 1.3
RCS J0220.9-0333	15	1.03	-0.010 ± 0.022	0.046 ± 0.012	14.9 ± 1.4
WARP J1415.1+3612 ³	12	1.03	-0.018 ± 0.020	0.022 ± 0.009	30.8 ± 0.9
RCS J2345.4-3632 ⁴	16	1.04	-0.050 ± 0.000	0.051 ± 0.011	24.5 ± 1.5
RCS J2156.7-0448 ⁴	7	1.07	-0.050 ± 0.000	0.098 ± 0.041	13.6 ± 1.4
RCS J0337.8-2844 ⁵	11	1.10	-0.108 ± 0.090	0.095 ± 0.032	18.6 ± 1.3
RDCS 0910+5422 ⁶	27	1.11	-0.044 ± 0.013	0.044 ± 0.009	21.5 ± 0.8
XLSS J0223.0+0436	18	1.22	-0.043 ± 0.022	0.048 ± 0.016	13.0 ± 1.1
RDCS J1252.9-2927 ⁶	19	1.24	-0.038 ± 0.011	0.027 ± 0.005	21.5 ± 0.7
RDCS J0848.9+4452 ⁶	23	1.27	-0.041 ± 0.009	0.034 ± 0.008	19.4 ± 0.5

¹ Number of E/S0 galaxies ($N_{E/S0}$), cluster spectroscopic redshifts (z_{spec}), observed $i_{775} - z_{850}$ CMR parameters.

² $N_{0.5}$: The GOODS background-subtracted number of galaxies within 2σ of the best-fit line (σ is our reported scatter) brighter than $0.3L_*$ at the cluster redshift, and within $0.5h^{-1}$ Mpc.

³ WARPS1415 X-ray detected cluster (Perlman et al. 2002).

⁴ A fixed slope is used to measure the scatter, the best-fit slope is sensitive to the color cuts used. See text.

⁵ Spectroscopic confirmation pending.

⁶ See Mei et al., 2009